Hindawi
Shock and Vibration
Volume 2022, Article ID 8975797, 14 pages
https://doi.org/10.1155/2022/8975797

Research Article

Damage Evolution of Granite under Ultrasonic Vibration with Different Amplitudes

Junpeng Han[1], **Dajun Zhao**[1], **Shulei Zhang**[2] **and Yu Zhou**[3]

[1]*College of Construction Engineering, Jilin University, Changchun 130026, China*
[2]*Yellow River Survey, Planning and Design Institute Co Ltd, Zhengzhou, Henan 450003, China*
[3]*Shaoxing University, Shaoxing, Zhejiang 312000, China*

Correspondence should be addressed to Dajun Zhao; 1690464517@qq.com

Received 26 January 2022; Accepted 16 August 2022; Published 31 August 2022

Academic Editor: Cristina Castejón

As a type of ultra-high frequency loading, ultrasonic vibration is an effective way to break the rock at high rates. Exploring the influence of various factors on the loading effect is essential for its effective application to assist drilling. In this study, the damage evolution of granite under ultrasonic vibration with different amplitudes was investigated. The theoretical and numerical simulation models of rock breaking by ultrasonic vibration were established. The research group applied ultrasonic vibration loading to granite using different amplitudes. The damage characteristics were tested by NMR experiment, and the damage evolution was numerical analyzed by Particle Flow Code software. The result shows that the propagation of cracks is positively correlated with the amplitude of ultrasonic vibration. The increase of amplitude magnifies the generation of transverse cracks, which is conducive to the stripping of rock fragments. A threshold value was found for the amplitude, and fractures show different propagation and expansion characteristics at the higher and lower values. Increasing the amplitude magnifies the stress at the crystal defect and speeds up the crack propagation process. The stress wave generated by ultrasonic vibration inside the rock will attenuate with the increase in depth. Increasing the amplitude value will amplify the stress in the influence area, and decrease the size of the area.

1. Introduction

With the development of mineral resources exploration, the demand for deep mining is increasing, which makes the drilling stratum come to be harder and harder. There is always a strong demand for efficient and rapid drilling in hard rock strata. Based on this, numerous scholars begin to search for new methods of rock crushing [1]. It is widely recognized that cyclic impact loading can cause fatigue failure inside the rock [2–4]. Accelerate the process of fatigue failure inside the rock by multiplying impact numbers per unit time, the rock breaking effect will be improved.

Ultrasonic vibration is a new type of rock crushing method that has received widespread attention in recent years. It is a kind of ultra-high frequency cyclic excitation, which is produced by the high-frequency reciprocating mechanical movement of piezoelectric materials using electric energy. Peng [5] analyzed the mechanism and energy propagation of drilling rock assisted by ultrasonic vibration. The experimental results show that the addition of ultrasonic vibration can significantly reduce the drilling pressure. Based on this advantage, some scholars try to use ultrasonic vibration technology in the process of extraterrestrial rock sample acquisition [6, 7]. Then some scholars put forward the rotary-percussive ultrasonic drill based on the structure of longitudinal torsional coupled vibration [7, 8]. This structure balances the rotation of drilling tools while maintaining longitudinal vibration, which improved the removal rate of rock chips. Several scholars have found that ultra-high frequency vibration can effectively reduce the compressive strength of rock, and cracks penetrating crystals were observed inside the rock after ultrasonic excitation [9]. Zhang [10] studied the mechanical properties of red sandstone under ultra-high frequency vibration and found that vibration with

high cycle rates can reduce the natural frequency and elastic modulus of rock samples. Fernando [11] studied the removal mechanism of rock materials in rotary ultrasonic machining and deduced a cutting force model to predict the relationship between input variables and cutting force.

Conditions of cyclic loading can affect the dynamic strength and fatigue life of rock [12, 13]. Haghgouei [14] proposed a damage model of rock materials, and the results show that the unsteady dynamic load amplitude has a great influence on the fatigue life of rock samples. The research of Yang [15] shows that rocks under constant amplitude and variable amplitude have different elastic and plastic deformation characteristics. Liao [16] established linear and nonlinear numerical models with excitation amplitude as the main control parameter to describe the dynamic process of rock drilling by vibration impact. Wang [17] studied the effect of loading frequency and amplitude on the fatigue properties of rock salt. The fatigue damage was found to be enhanced with the increase of stress amplitude and the decrease of loading frequency. The residual strain tends to decrease with the rising value of amplitude in cyclic loading [18], this variable can well reflect the degree of rock damage [19]. Wang [20] analyzed the damping characteristics of rock under cyclic loading and considered that the order of influence effect in parameter indexes from strong to weak should be stress, amplitude, and frequency. Geranmayeh [21] found in the cyclic compression experiment that increasing the loading amplitude can cause more lateral damage evolution inside the rock. Zhou [22] deduced the function of permeability evolution, which verified the influence of force amplitude and frequency on cracks, and found that blindly enhancing the amplitude cannot continuously enhance the penetration and propagation of cracks. There is an optimal range for the amplitude value of the load [23]. The propagation of stress waves in rock will appear amplitude attenuation, which is largely affected by rock heterogeneity [24].

Although the effect of amplitude on the cycle loading has been studied at a certain level in previous research, the loading frequency selected in most cyclic loading studies remains at a small value. The mechanism of rock breaking under ultrasonic vibration is relatively lacking. The cyclic loading of ultrasonic vibration is rarely covered, lacking a detailed description of the influence trend of amplitude. It is necessary to conduct in-depth research on the influencing factors of ultrasonic vibration. In this study, we applied ultrasonic vibration to granite with different amplitudes. Nuclear magnetic resonance scanners were used to detect damage characteristics of granite. A two-dimensional model was established by Particle Flow Code software to simulate the rock damage evolution process. Based on simulation and experimental results, the mechanical behavior, fracture evolution, and fracture orientation were analyzed. The influence of amplitude on ultrasonic vibration was discussed, and the optimal parameter interval was found.

2. Experimental Methods

2.1. Sample Preparation. The granite sample selected for the experiment is a kind of medium-grained granite quarried from one mine in Jilin Province, China. The physical and mechanical parameters of the granite in the natural state were measured experimentally: density 2.79 g/cm3, elastic modulus 29.8 GPa, Poisson's ratio 0.22, uniaxial compressive strength 98.75 MPa. The test sample is cylindrical granite with a diameter of 35 mm and a height of 70 mm obtained from the same rock by the XY-1 drilling rig. The upper and lower surfaces of the sample are polished to control the flatness and parallelism of both sides. The selection of sample diameter and height meets the requirements of the ISRM standard. The major mineral compositions and proportions of the rocks include alkali feldspar (45%), plagioclase (17%), quartz (31%), and mica (7%).

2.2. Test Device and Setting. The equipment used in the experiment is shown in Figure 1, including loading and testing parts. As for the loading device, the ultrasonic power source generates a high-frequency alternating current, which is transmitted to the ultrasonic vibrator through the wire and drives the piezoelectric ceramic plate to generate ultrasonic vibration. The resulting ultra-high frequency micro-stroke reciprocating motion is transmitted and applied to the rock sample below the vibrator after amplifying the amplitude by the horn. Counterweight blocks are placed at the top of the vibrator, transmitting force down through the bracket to apply static loads to the rock. A timer is used to precisely control the ultrasonic vibration loading on the rock sample. As for the testing equipment, the pressure saturation device is used to finish the water saturation operation on rock samples, so that the water molecules can abundantly fill into fractures. 'MesoMR' nuclear magnetic resonance scanner is used to scan the rock, in order to detect and count the number of cracks inside the rock, collecting test data into the computer.

The static load set during the experiment is 200 N, the frequency generated by the ultrasonic vibrator is 30 kHz, the excitation amplitude is 40 μm, and the amplitude can be switched between 50% and 100%. In this experiment, we selected six vibration amplitudes in the range of 50%–100% at equal intervals, with five samples per group to exclude individual errors. All tests were conducted at room temperature, and all other conditions were kept constant.

3. Experimental Results

3.1. Porosity Evolution. The porosity of rock before and after ultrasonic vibration with different amplitudes was statistically collated. Figure 2 shows the changes in the average porosity of six groups of rock samples during the test. It can be found that applying ultrasonic vibration to the rock increases the rock porosity, no matter how big the amplitude value is. This is due to the original cracks inside the rock having been stretched under the action of the high-frequency cyclic load of ultrasonic vibration. As the value of amplitude becomes larger, the increase in rock porosity after ultrasonic vibration comes to rise accordingly. In the process of increasing amplitude values, a leaping transition can be observed in the rock porosity. When the amplitude value

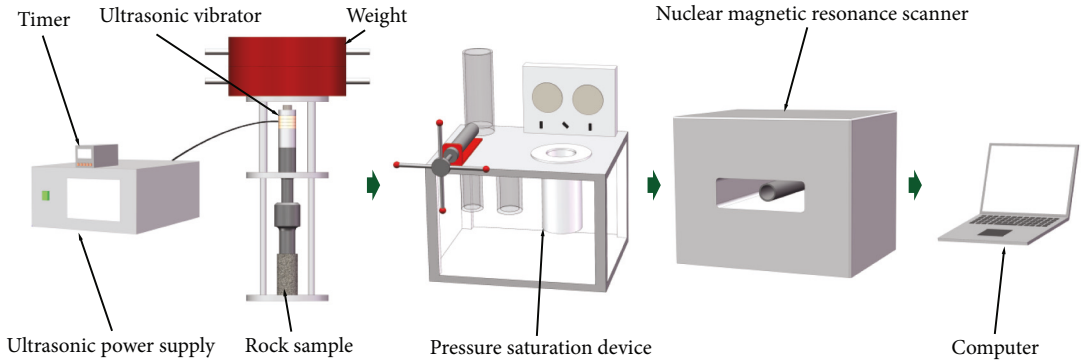

Figure 1: Test equipment and process.

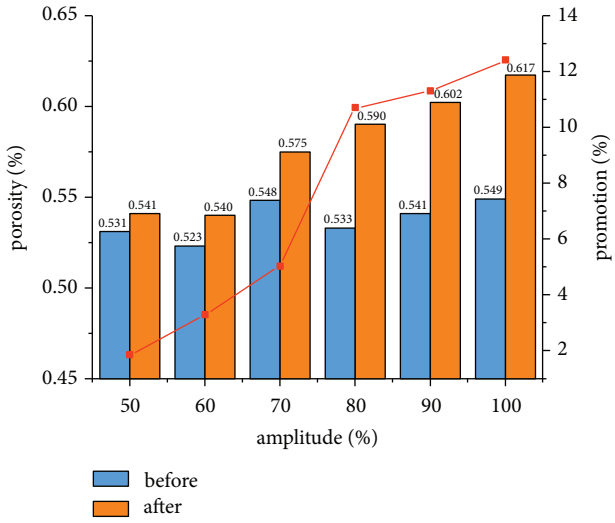

Figure 2: Average porosity before and after vibration.

increases from 70% to 80%, the increase in porosity is significantly higher than that corresponding to the other two adjacent amplitude values.

3.2. T2 Spectrum. In NMR detection, the size of the pore diameter shows a positive correlation with the value of the relaxation time in the obtained T2 spectrum, and the area of the spectrum enclosed by the curve represents the pore volume in the current range of the pore size [25]. For this reason, the T2 curve can demonstrate the change of pore structure inside the rock before and after the application of ultrasonic vibration.

The a–f in Figure 3 respectively correspond to the six experimental groups with vibration amplitude values ranging from 50% to 100%. Figure 3(a) shows that the first and second peaks in the T2 spectrum have an obvious tendency to shift toward the right, with a decrease in the volume of micro-pores and an increase in the volume of medium-size pores. The area of the third peak decreases but the curve shifts significantly to the right, corresponding to the creation of a small part of large-size pores. The whole curve indicates that one part of the original cracks is compacted after ultrasonic vibration, while the other part expands and develops into medium-size cracks. Parts of large cracks are compacted into medium and small cracks after vibration, while the other part transforms into larger cracks. Medium size is the dominant form of the newly generated cracks. The dilation of small-size cracks and the proliferation of medium-size cracks can be seen more significantly in Figure 3(b). When the amplitude value reaches a certain scale, the closure of the microcracks due to the compaction of the cyclic load is overcome and more microcracks are generated (Figure 3(c)). The scale of new small-size crack generation is more significant after increasing amplitude (Figures 3(d) and 3(f)), while the expansion and propagation of medium-size cracks are the main trends at relatively small amplitude values (Figures 3(a)–3(c)).

3.3. Crack Evolution. Figure 4 shows the distribution ratio of cracks inside the rock under different amplitudes calculated by the analysis software, and a-f corresponds to six experimental groups with vibration amplitudes of 50%–100%. It can be seen that the percentage of cracks with a pore size less than 0.25 μm in groups *a*, *b*, and *c* have different degrees of reduction after ultrasonic vibration. And the percentage of cracks with pore size between 4 μm and 16 μm is significantly increased after vibration. while the cracks of this pore size consistently maintain a higher proportion in the groups *d*, *e*, and *f*. The proportion of cracks with sizes less than 1 μm in these three groups exhibits various degrees of improvement after vibration.

Referring to Liu [26], the crack inside the rock can be divided into three types based on the pore size. The pore size of type I is less than 1 μm, type II has a size between 1 μm and 10 μm, and the crack with a pore size bigger than 10 μm is type III. Figure 5 shows the changes in the number of type I, II, and III cracks before and after ultrasonic vibration in the six experimental groups.

Figure 5(a) shows the volume proportions of the three types of cracks before and after ultrasonic vibration, and Figure 5(b) shows the corresponding porosity values of the three types of cracks. From the above figure, it can be seen that after the ultrasonic vibration with 50% and 60% amplitude, the type I cracks inside the rock has been significantly reduced, while the type II cracks have a remarkable increase. So under the excitation of cyclic loading with this

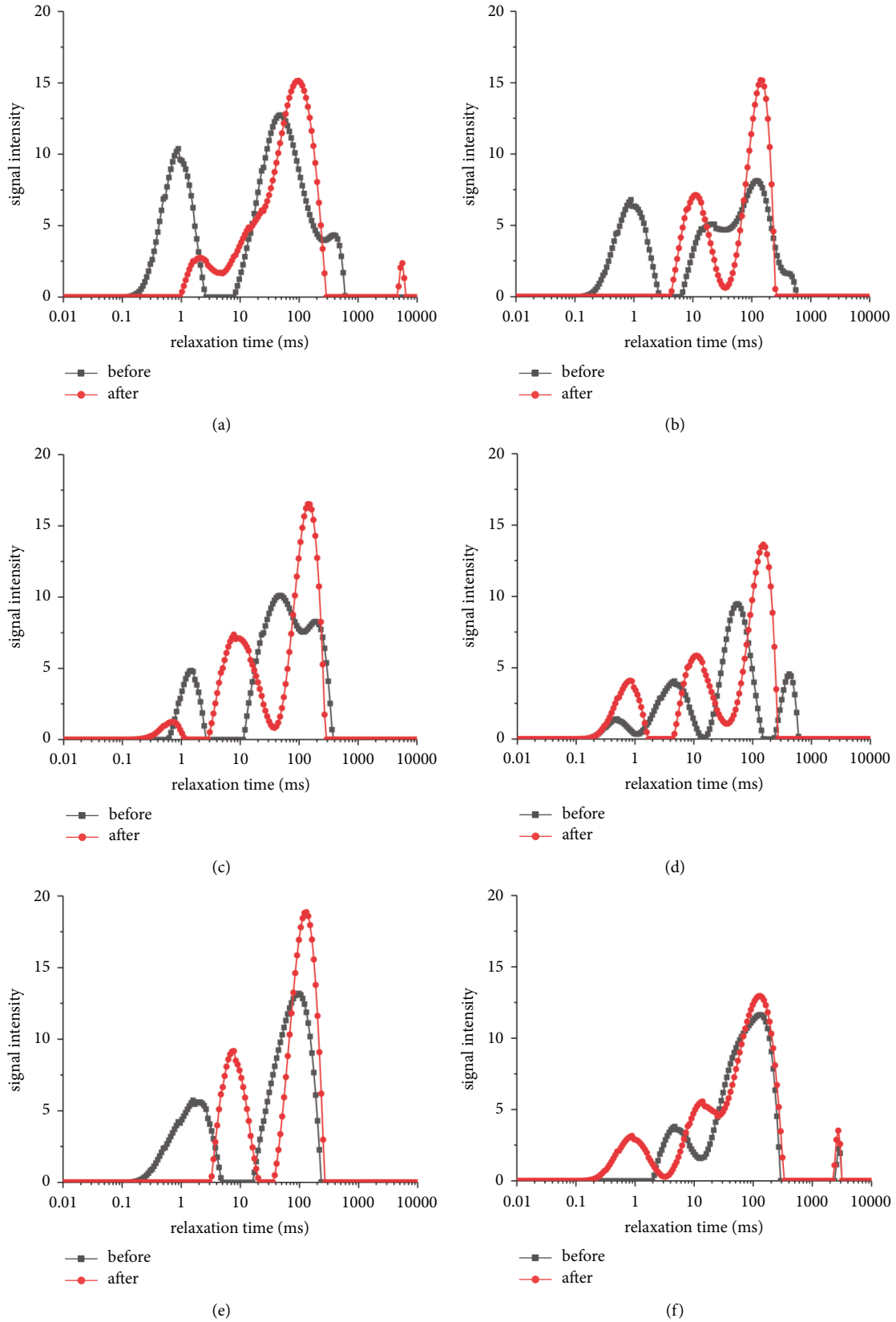

Figure 3: T2 spectrum before and after ultrasonic vibration under different amplitudes: (a) 50%, (b) 60%, (c) 70%, (d) 80%, (e) 90%, (f) 100%.

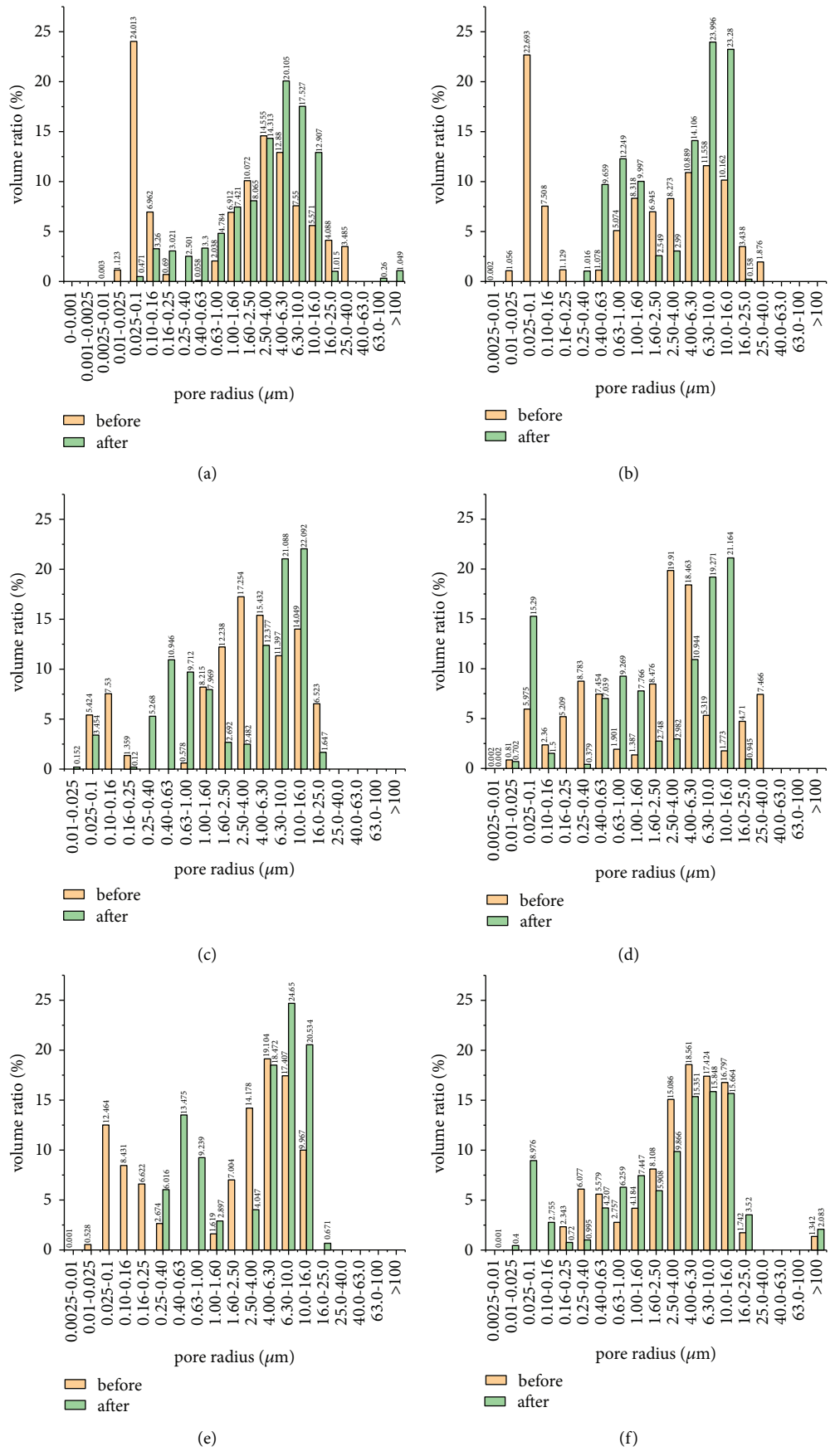

Figure 4: Pore size distribution before and after vibration at different amplitudes: (a) 50%, (b) 60%, (c) 70%, (d) 80%, (e) 90%, (f) 100%.

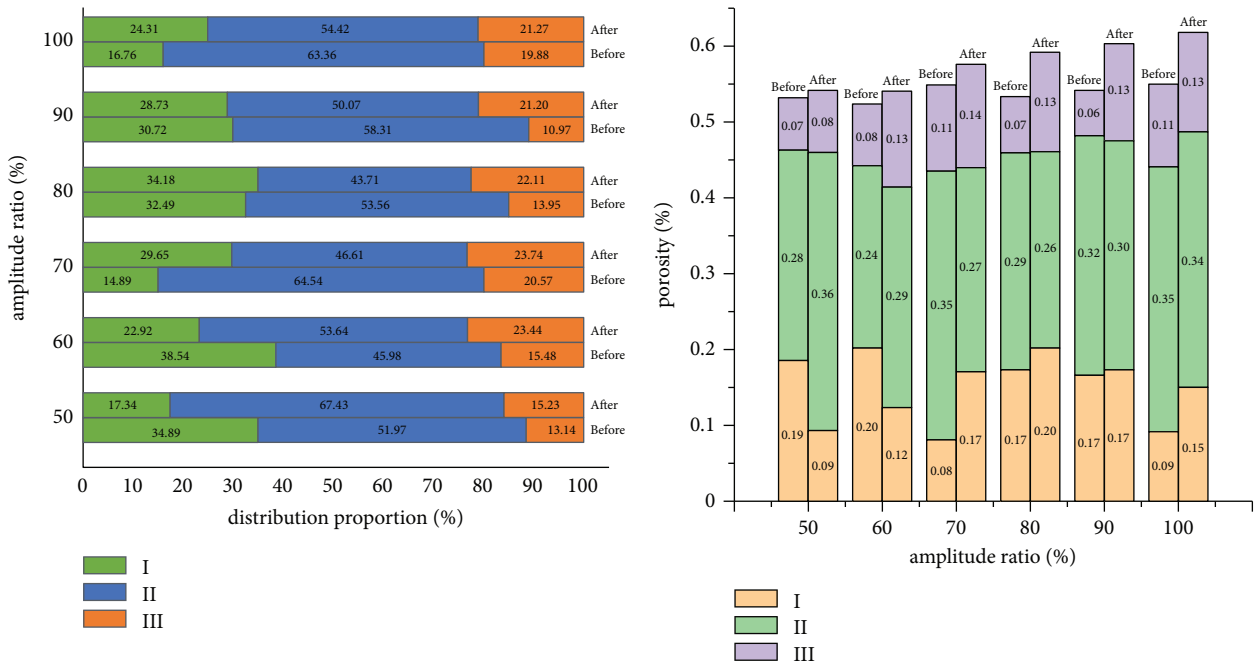

Figure 5: Percentage and value of porosity of three types of pores: (a) the percentage of pores, (b) porosity of pores.

amplitude, the main tendency of the original cracks inside the rock is the expansion and development of small-size cracks to medium-size fractures, and few microfractures will be generated. The four experimental groups with amplitude values ranging from 70% to 100% all show the same tendency of fracture change, that is, type I and type III cracks increase, and type II cracks decrease. This indicates the effect of ultrasonic vibration on the tendency of crack development in these four groups that new microcracks are propagated on a certain scale, and the vibration drives the transformation of medium-size cracks to large ones. However, the group with 70% amplitude has a different performance from the latter three experimental groups. The increase of type III cracks is smaller than the decrease of type II cracks, which should be due to the cyclic compression of ultrasonic vibration that makes some of the pores closed, resulting in a certain degree of volume reduction of some cracks. Therefore, the amplitude of 80%, 90%, and 100% has more positive significance in promoting crack development.

4. Construction of Numerical Simulation Model

The discrete unit analysis method of particle flow code forms the research object by combining multiple spherical particles that can produce independent motion with contact definition, and obtain force and displacement data through iterative calculation. This has more obvious advantages in studying dynamic damage and micro-crack development in rock materials.

4.1. Theoretical Model. Before the numerical simulation, a basic analysis of the interaction process between tools and rock samples should be carried out. Reasonable simplification of the process of rock breaking by ultrasonic vibration can facilitate the establishment of the corresponding theoretical model and the derivation of the motion equation. The premise of simplification is to determine basic assumptions. In this study, we assume that the ultrasonic vibration structure is a rigid body, ignoring the influence of the clearance. The simplified model is shown in Figure 6.

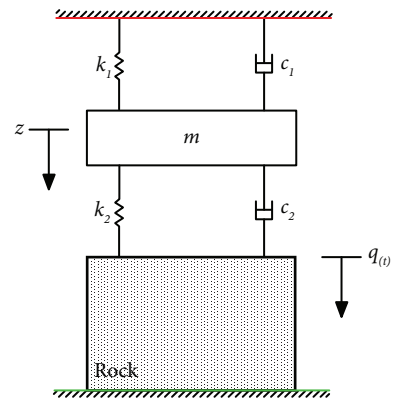

Figure 6: Simplified model of rock breaking by ultrasonic vibration.

According to Figure 6, the equation of motion can be established:

$$m\ddot{z} = -k_1 z - c_1 \dot{z} + k_2 (q(t) - z) + c_2 (\dot{q}(t) + \dot{z}) + mg, \quad (1)$$

where m is the mass of the ultrasonic vibrator, z is the displacement of the ultrasonic vibrator, k_1 is the stiffness of the force transfer frame, c_1 is the damping of the force

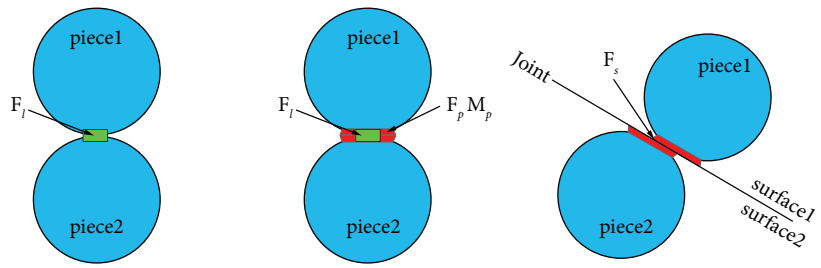

Linear Model Linear Parellel Bond Model Smooth-Joint Contact Model

Figure 7: Contact model mechanism.

transfer frame, $q(t)$ is the displacement of the rock surface, k_2 is the stiffness of ultrasonic vibrator, c_2 is the damping of ultrasonic vibrator damping.

The displacement of the ultrasonic vibrator can be expressed by:

$$z = A\sin(2\pi ft), \tag{2}$$

where A is the amplitude of ultrasonic vibration, m; f is the frequency of ultrasonic vibration, and Hz; t is the time, s.

According to the vibration theory, the vibration system with a single degree of freedom will produce a vibration response with the same frequency under the excitation of simple harmonic vibration. The period of the impact system and the response system is consistent, but the displacement does not reach its maximum at the same time. There is a phase difference between the two systems. The dynamic response is generated inside the rock under the action of ultrasonic vibration. The displacement equation of rock surface is: [27].

$$q(t) = A'\sin(2\pi ft - \varphi), \tag{3}$$

where A' is the amplitude of dynamic response, and φ is the phase difference between rock and vibrator.

$$\dot{z} = 2\pi fA\cos(2\pi ft), \tag{4}$$

$$\ddot{z} = -4\pi^2 f^2 A\sin(2\pi ft), \tag{5}$$

$$\dot{q}(t) = 2\pi fA'\cos(2\pi ft - \varphi). \tag{6}$$

Substituting (2)–(6) into (1) can get:

$$A' = \frac{A\left[\left(k_1 + k_2 - 4m\pi^2 f^2\right)\sin(2\pi ft) + 2\pi f\left(c_1 + c_2\right)\cos(2\pi ft)\right] + mg}{k_2\sin(2\pi ft - \varphi) + 2\pi fc_2\cos(2\pi ft - \varphi)}. \tag{7}$$

It can be seen that the response amplitude of rock magnifies with the increase of the amplitude of the ultrasonic vibrator. The stress waves inside the rock start with the response amplitude of the rock surface. The displacement generated by the transfer of force between the mineral crystals realizes the propagation of the stress wave, and finally produces damage in the rock.

4.2. Numerical Simulation Model. The particles and walls are the main elements in the particle flow code and are interconnected by contact for the transmission of forces and torques. The contact model is the definition of the interaction mode between particles, which correlates the relative motion of particles at the contact with the generalized internal force. The calculation of generalized internal forces given by different contact models varies, and each type of model has its unique conditions of application. The linear model provides linear elastic friction with viscous behavior acting on a vanishingly small area, which makes it capable of transmitting only force but not torque. Tension is not able to be transmitted here either. The linear parallel bond model is frequently used to simulate crack extension in rock materials [28–30]. It establishes elastic interactions that are uniformly distributed over the surface between contacts. The relative motion occurring at the contact will cause forces and torques. When the stress value exceeds the bond strength, the bond will be broken and only linear and damping forces remain between the particles. The smooth-joint model can simulate the crack behavior of the grain interface [31]. It provides the mechanical behavior of the friction interface without interference from the contact direction of local particles, and the bonded interface is endowed with linear elastic properties. When the applied force exceeds the cohesive strength causing the failure of the bond, the particles slip on the bonding surface under the influence of shear force. Based on this feature, frictional behavior can be represented. Figure 7 shows the interaction forms of the three contact models between particles.

As a kind of magmatic rock with phanerocrystalline texture, the various mineral crystals within granite have different mechanical properties. In the process of numerical simulation, the Gaussian function is applied to randomly generate particles of 0.5–0.7 mm in diameter (Figure 8(a)).

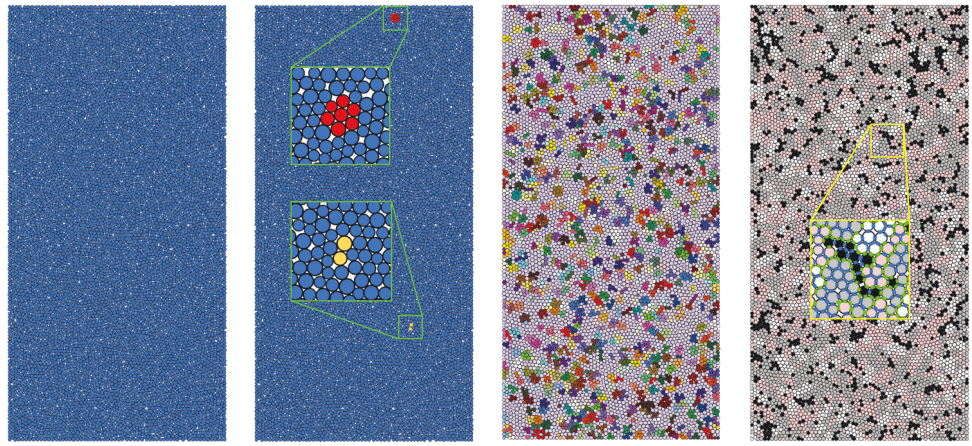

(a) (b) (c) (d)

Figure 8: Numerical simulation model of granite: (a) Initial particle set, (b) particle cluster generation, (c) model with particle clusters, (d) models with mineral grouping.

Table 1: Micro-parameters of granite model.

Property	Quartz	Mica	Plagioclase	Alkali feldspar
Particle				
Density ρ (kg/m^3)	2650	2800	2630	2630
Linear model				
Effective modulus E_L^* (GPa)	10	10	10	10
Normal critical damping ratio β_{nL}	0.5	0.5	0.5	0.5
LPB model				
Effective modulus E_{LP}^* (GPa)	60	20	40	35
Normal-to-shear stiffness ratio k_{LP}^*	2.5	2.5	2.5	2.5
Friction coefficient μ_{LP}	0.6	0.6	0.6	0.6
Bond effective modulus $\overline{E}_{LP}^*$ (GPa)	60	20	40	35
Bond normal-to-shear stiffness ratio $\overline{k}_{LP}^*$	2.5	2.5	2.5	2.5
Tensile strength $\overline{\sigma}_{cLP}$(MPa)	500	300	400	400
Cohesion $\overline{c}_{LP}$(kN)	1000	600	800	800
Friction angle $\overline{\varphi}_{LP}$ (°)	35	25	30	30
SJ model				
Normal stiffness k_{nSJ} (GPa)	$0.6 \times k_{nLP}$	$0.6 \times k_{nLP}$	$0.6 \times k_{nLP}$	$0.6 \times k_{nLP}$
Shear stiffness k_{sSJ} (GPa)	$0.6 \times k_{sLP}$	$0.6 \times k_{sLP}$	$0.6 \times k_{sLP}$	$0.6 \times k_{sLP}$
Tensile strength σ_{SJ} (MPa)	12	12	12	12
Cohesion c_{SJ} (kN)	120	120	120	120
Joint friction angle φ_{SJ} (°)	30	30	30	30

The clusters are generated one by one using the particles extend cluster method (Figure 8(b)) until the entire model is plenty filled (Figure 8(c)). The clusters are randomly grouped according to the mineral proportions using a random function, and eventually, all particles are assigned to four groups: alkali feldspar (45%), plagioclase (17%), quartz (31%), and mica (7%) (Figure 8(d)). Micro parameters such as modulus of elasticity, normal to tangential stiffness ratio, friction angle, and cohesion are set separately for each group according to the actual conditions of the mineral crystals. The microscopic parameter values of each kind of mineral are shown in Table 1. The linear parallel bond model is set within each mineral crystal (blue line in Figure 8(d)), and the smooth-joint model is set between two separate mineral crystals to simulate the frictional and slip properties between crystals (green line in Figure 8(d)).

4.3. Parameter Calibration. In the numerical simulation, it is necessary to calibrate the constructed numerical model to obtain real simulation results. According to the macro mechanical parameters of the specimen obtained from the indoor uniaxial compression experiments, the micro parameters are adjusted to make the test and simulation show the same characteristics.

Laboratory uniaxial compression tests and numerical simulations based on the same sample size are carried out simultaneously. Uniaxial compression test was carried out according to ISMR standard, and the tested rock sample was selected as Φ 35 mm × 70 mm granite column. The microscopic parameters of the rocks in the discrete element model are adjusted by the trial-and-error method so that the simulation and the test have closer characteristics. The uniaxial compression experiment and simulation results are

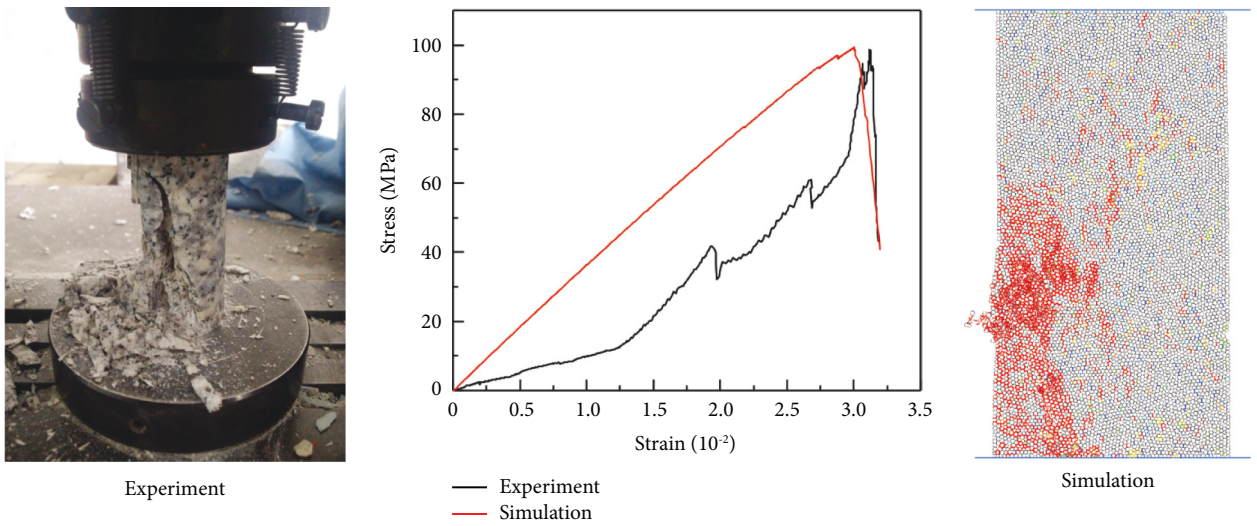

Figure 9: Uniaxial compression results of experiments and numerical simulations.

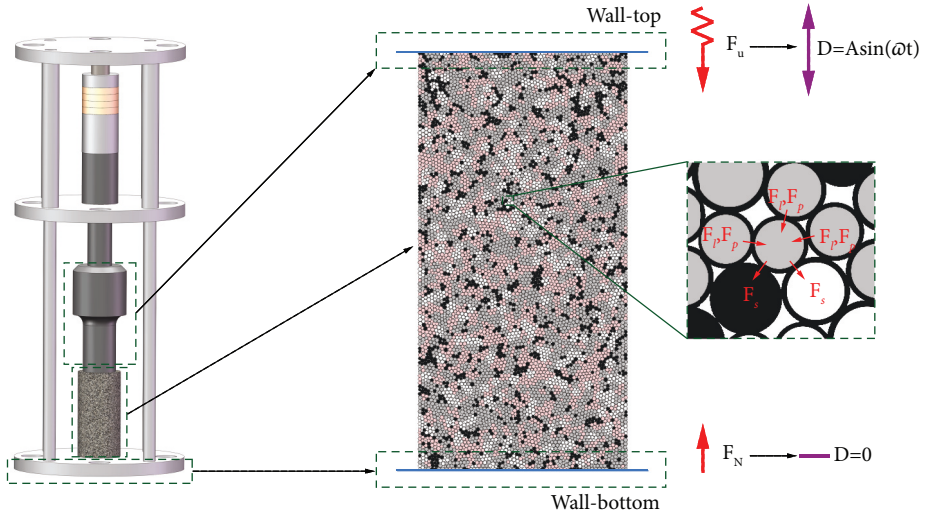

Figure 10: Model loading conditions corresponding to the experiment.

shown in Figure 9. After parameter calibration, the stress-strain curve obtained by numerical simulation and the stress-strain curve obtained by test have similar fluctuations and peaks, and the same rock damage characteristics appear in both test and numerical simulation.

4.4. Loading Condition. The model data obtained in the parameter calibration process are applied to the numerical simulation model of rock breaking by ultrasonic vibration. Figure 10 shows the loading conditions and the force transfer process of the model corresponding to the experiment.

The loading for ultrasonic vibration is achieved by assigning a state of motion to the top wall which is close to the variation trend of the sinusoidal curve. The displacement of the top wall at any moment is:

$$y = A \bullet \sin(2\pi f t). \tag{8}$$

Convert it to the corresponding speed v_y :

$$v_y = A \bullet 2\pi f \cos(2\pi f t). \tag{9}$$

The bottom of the apparatus carrying the rock during the test is a fixed boundary, then the corresponding bottom wall velocity in the numerical simulation model is set to change according to conditions. When the static pressure on the rock is detected to be 200 N, the wall speed is assigned to 0, otherwise, it will move upwards at an extremely small speed to make the pressure on the rock reach the target value.

5. Mechanical Behavior and Fracture Evolution

5.1. Force Behavior. Contact is the bridge between particles and is also the medium of force transmission. The numerical simulation model of granite is formed by bonding particles with contacts, so the examination of the forces in contact between the particles can show the stress state inside the

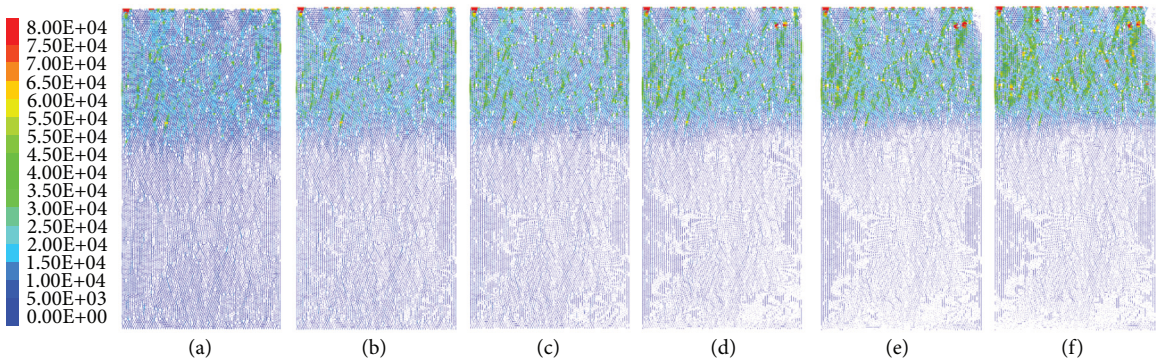

Figure 11: Contact force distribution under different amplitudes: (a) 50%, (b) 60%, (c) 70%, (d) 80%, (e) 90%, (f) 100%.

rock. The distribution trend of contact forces is approximately the same for different amplitude values of ultrasonic vibration loading conditions (Figures 11(a)–11(f)). The stress distribution area with a high value has a certain depth range and cannot extend downward indefinitely. With the increase of the amplitude, the stress value shows a rising trend, while the distribution area decreases slightly. Stress concentrations start to appear in some natural defect areas.

5.2. Fracture Evolution. In the numerical simulation of rock, the discrete fracture network is a common way to measure and characterize the development of rock fractures [32]. Figure 12 shows the number and distribution of discrete fracture networks inside the rock under different amplitude conditions. It can be found that the number of fractures grows with the increase of amplitude, and there is a transition value in this enhanced process. The promotion effect of vibration on crack extension is most significantly enhanced at the amplitude of 80%. The overall trend of the promotion effect appears to be a slow increase initially and eventually, with a sharp increase occurring in the middle. However, the gain effect improvement rate in the latter half is significantly higher than that in the first half, which has the same trend as the porosity measured during the test. From the fracture distribution diagram, it can be found that ultrasonic vibration has a certain range of limits on the development depth of rock fractures. The change of amplitude value has little effect on the working depth of ultrasonic vibration inside the rock. Increasing the amplitude can generate more fractures in the shallow area at a certain depth below the rock surface, which will be more conducive for the shallow rock to produce fragments and peel off the rock body.

5.3. Fracture Orientation. The rose diagram is an excellent tool for showing and summarizing the azimuth angle of fractures inside the rock. Figure 13(a) and 13(b) respectively shows the azimuthal information of fractures inside the rock after ultrasonic vibration in six experimental groups with amplitude values of 50%–100%. The values of the peripheral circumferential coordinates in the figure represent the azimuth of the fracture, and the inner circular contours represent the intensity of the fracture. The frequency of

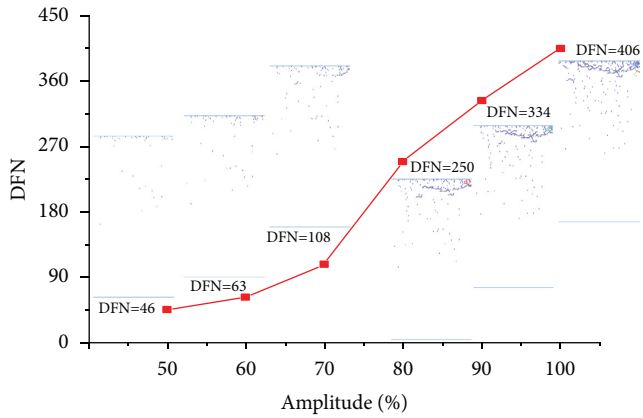

Figure 12: Discrete rift network at different amplitudes.

fracture formation at each azimuth is reflected by the length of each petal.

No matter how much the amplitude is, fractures inside the rock mainly propagate in the vertical (90°) direction under the loading of ultrasonic vibration. By increasing the amplitude of ultrasonic vibration (Figures 13(d)–13(f)), more inclined fractures in the rock can be observed, which is of positive significance for the generation and stripping of rock fragments. The orientation of newly generated lateral fractures is mainly at 30° and 120°, and this tendency is more obvious under loading conditions with larger amplitudes (Figure 13(f)). And when the load amplitude takes a smaller value, the fractures generated by the vibration are basically in the vertical direction, and almost no lateral fractures are observed.

6. Discussion

In one loading cycle, the rock experiences the compression of stress impact and the rebound of stress release. The difference in mechanical parameters between the mineral crystals of rock leads to stress concentration at the contact and develops into local defects, which is the primary crack in the natural state of rock (Figure 14(a)). Ultrasonic vibration is a process of cyclic load with an extremely small period. In the first half of one cycle, the impact body at the forefront of the vibrator strikes the rock with kinetic energy, causing the

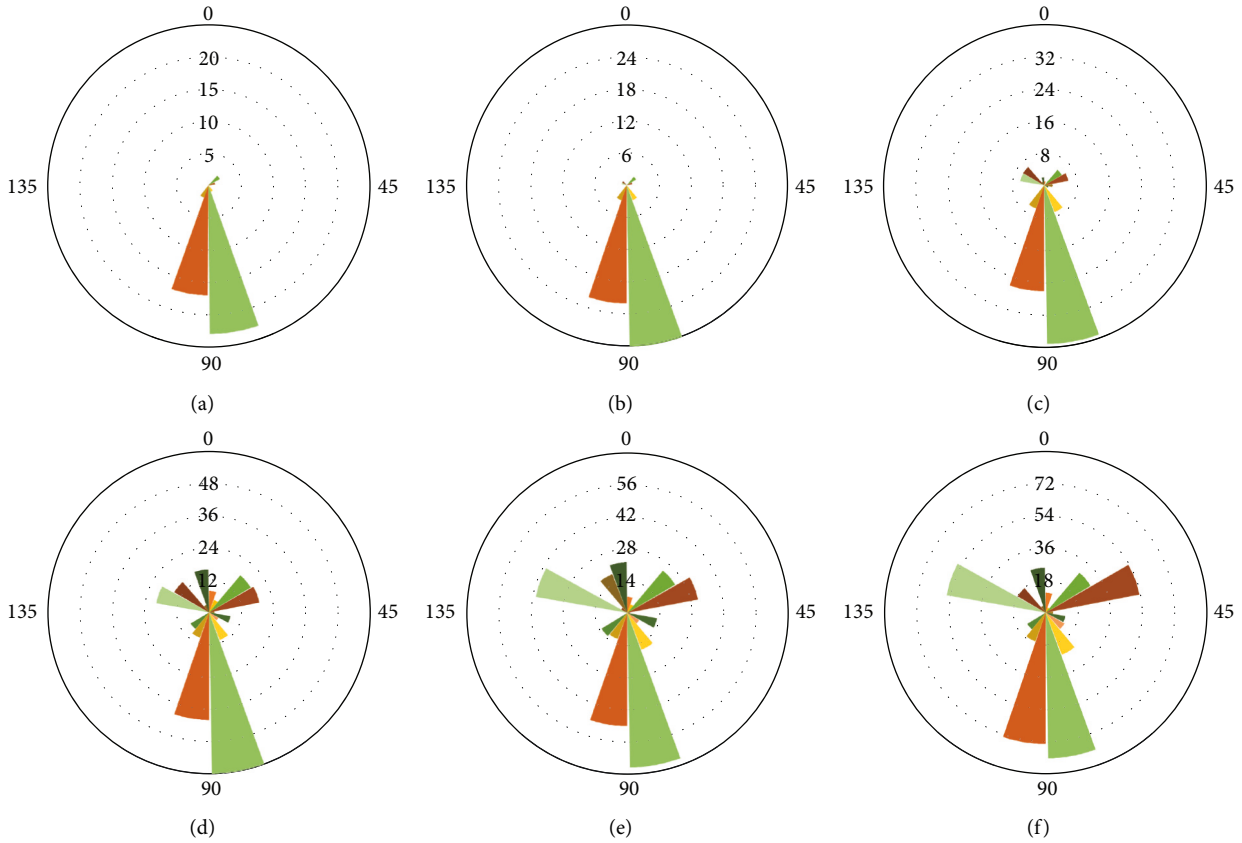

Figure 13: Distribution of crack orientation under different amplitudes: (a) 50%, (b) 60%, (c) 70%, (d) 80%, (e) 90%, (f) 100%.

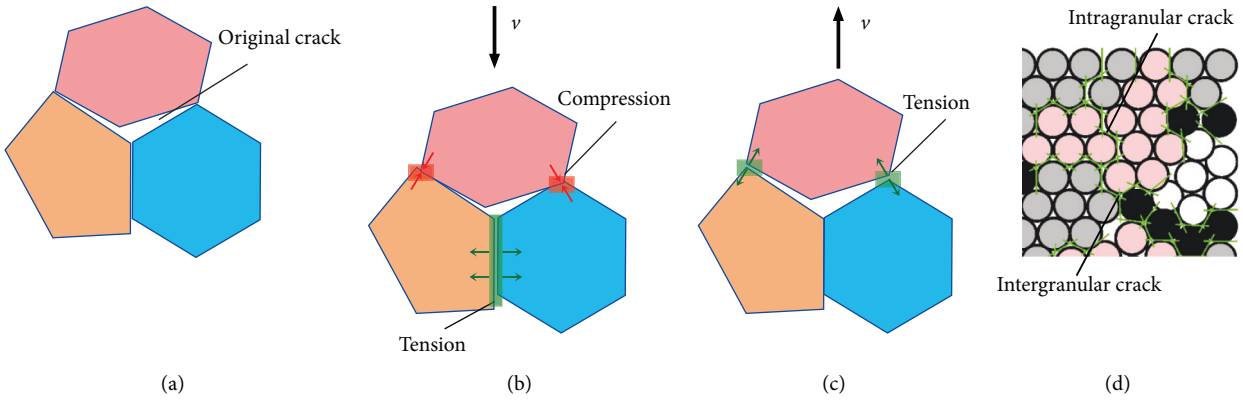

Figure 14: Crystal and crack changes under cyclic loading: (a) initial state, (b) stroke stage, (c) return stage, (d) simulated crack distribution between crystals.

displacement of shallow mineral crystals. Compressive and tensile forces will be generated at the crystal junction and the original natural cracks within the rock will be closed (Figure 14(b)). The return stroke of the impact body in the second half cycle causes pressure on the crystal to be replaced by tension. And the rock with elastic-plastic properties springs back, resulting in the cracks rebounding and expanding after the pressure is released (Figure 14(c)). In the high-frequency periodic shape change, the tension and compression change alternately, leading the fatigue failure easy to occur here. The alternating load tends to produce cracks at the crystal boundary, where the strength is usually weak. Cracking can also occur inside relatively weak crystals. The uneven stress applied to the mineral crystal particles results in stress concentration inside the crystal, and the original defects in the crystal expand to form cracks. These kinds of cracks tend to occur in quartz and feldspar. The magnitude of the amplitude determines the stroke of the impact body in the cycle. Therefore, the displacement of mineral crystals is affected, which is also the deformation of

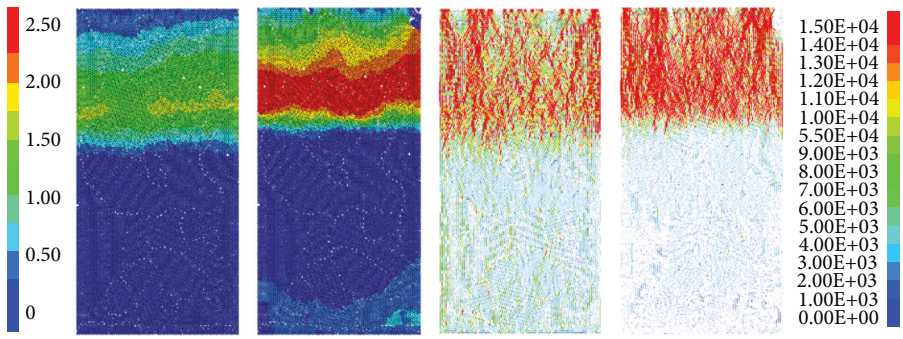

Figure 15: Instantaneous velocity and stress distribution: (a) instantaneous velocity of particles with 50% amplitude, (b) instantaneous velocity of particles with 100% amplitude, (c) stress distribution with 50% amplitude, (d) stress distribution with 100% amplitude.

crack closure and expansion. Larger deformations represent a more intense stress concentration at the crack tip. The permanent expansion of the cracks subsequently occurs, which is manifested in the macrography as an increase in the porosity of the rock.

According to the previous study results of the research group, the rock under ultrasonic vibration loading can be characterized by three stages: crack closure, crack initiation and propagation, and large fracture formation [33]. The stage of the rock will also show differences at different loading parameters. When the amplitude is lower than the threshold, the number of type I cracks decreases obviously after vibration, while the total number of cracks increases slightly. This indicates that the crack initiation and propagation stage and the crack closure stage coexist in the rock. After reaching the threshold, the number of type I and type III cracks increases and the number of type II cracks decreases slightly, which indicates that the initiation and propagation of new cracks and large fracture formation coexist in the rock. The experimental results show a decrease in the number of micro-pores with diameters less than 1 μm at loading amplitudes below 70%. On the one hand, it is due to the expansion of micro-cracks to form larger-size cracks. On the other hand, the rock is accompanied by rock chips under the action of alternating loads, and the transport of fallen rock chips may cause the blockage of cracks. The number of micro-pores increases only after the amplitude reaches the threshold.

The cyclic load is applied to the rock mainly in the form of kinetic energy and propagates downward as a stress wave. Kinetic energy transfer between mineral crystals is the pathway for the downward propagation of stress waves. The heterogeneity of rock has a great influence on the amplitude attenuation of stress waves [24]. Cai [34] believes that cracks in the rock will interfere with the diffraction and reflection of stress waves in transmission. The fluctuating displacement of the crystal under stress is accompanied by the generation of frictional heat, which creates a drain on the energy of the stress wave. In previous research, we explored the damage characteristics of granite under ultrasonic vibration through a thermal imager, and concluded that the friction heat energy generated by ultrasonic vibration in rock is greater than that consumed by microcracks cracking. Granite is heterogeneous and contains mineral particles with different thermal expansion coefficients and thermoelastic properties. The accumulated high temperature causes uneven thermal expansion of mineral particles and phase transformation of minerals, which will lead to inner stress gradients in rocks, promote crack development and cause thermal damage. [35]. In the process of impact, part of the energy is absorbed by the rock. The energy gathered at the original tiny defects in the rock stimulates the formation of cracks. [36] Finally, the energy is released during the generation of cracks and fragments, which makes the stress wave energy consumed. The differences in the physical and mechanical properties of mineral particles make it easy for ultrasonic waves to gather and diffract with the change of the medium during the propagation process. The energy also dissipates quickly in the process. An energy gradient can be observed inside the rock. For these reasons, ultrasonic vibration causes obvious heterogeneous damage at different positions of rock. Therefore, the energy of the stress wave decreases with the increase of rock depth. The distribution tendency of contact force in Figure 11 directly reflects the attenuation characteristics of stress waves with rock depth. Figure 15 compares the instantaneous velocity of particles and stress distribution under loading conditions with 50% and 100% amplitude. This also verifies in the simulation process, the influence of ultrasonic vibration load on the rock has a certain depth range. The increase of amplitude value enlarges the reciprocating stroke in unit time. The impact body requires increasing velocity to complete a longer stroke at the same time, which means the acceleration of the crystal becomes bigger. The stress that produces acceleration shows the same trend. More intense collisions produce more energy loss. Therefore, increasing the amplitude reduces the stress in the deep region and increases the stress in the shallow layer, and the range of the high-stress region decreases.

7. Conclusion

In this study, the damage evolution of granite under ultrasonic vibration excitation with different amplitude values was investigated. The theoretical and numerical simulation models of rock breaking by ultrasonic vibration were established. Laboratory tests of applying ultrasonic vibration

to granite samples using different amplitude values were carried out. The damage characteristics of granite were tested by NMR experiment, and the damage evolution process was analyzed by Particle Flow Code software. The following conclusions are drawn.

The propagation of cracks is positively correlated with ultrasonic amplitude. A threshold can be found in the amplitude values, above which the rock porosity shows a leaping growth. Below the threshold value, the interior of rock tends to expand cracks, while above this value, the formation of new cracks and the penetration failure of large cracks tend to occur. Transverse cracks conducive to the stripping of rock fragments are also more likely to be generated.

The periodic displacement of rock mineral crystals is the cause of crack propagation in the rock under ultrasonic vibration. Increasing the amplitude magnifies the stress at the crystal defect and speeds up the crack propagation process.

The stress wave generated by ultrasonic vibration in the rock will attenuate with the increase of depth. The influence of ultrasonic vibration on rock has a depth range. Increasing the amplitude value will amplify the stress in the influence area, and decrease the size of the area.

Data Availability

The data used to support the findings of this study are included in the article.

Conflicts of Interest

The authors declare that there are no conflicts of interest regarding the publication of this paper.

Acknowledgments

This research was funded by the National Natural Science Foundation of China, grant no. 4157020248.

References

[1] F. Gao, Y. Shao, and K. Zhou, "Analysis of microwave thermal stress fracture characteristics and size effect of sandstone under microwave heating," *Energies*, vol. 13, no. 14, Article ID 3614, 2020.

[2] Y. Liu, F. Dai, L. Dong, N. Xu, and P. Feng, "Experimental investigation on the fatigue mechanical properties of intermittently jointed rock models under cyclic uniaxial compression with different loading parameters," *Rock Mechanics and Rock Engineering*, vol. 51, no. 1, pp. 47–68, 2018.

[3] M. N. Bagde and V. Petros, "Fatigue properties of intact sandstone samples subjected to dynamic uniaxial cyclical loading," *International Journal of Rock Mechanics and Mining Sciences*, vol. 42, no. 2, pp. 237–250, 2005.

[4] S. Huang, K. Xia, and H. Zheng, "Observation of microscopic damage accumulation in brittle solids subjected to dynamic compressive loading," *Review of Scientific Instruments*, vol. 84, no. 9, Article ID 093903, 2013.

[5] X. Peng, L. Li, Y. Yang, G. Zhao, and T. Zeng, "Experimental study on rotary ultrasonic vibration assisted drilling rock," *Advances in Space Research*, vol. 67, no. 1, pp. 546–556, 2021.

[6] X. Bao, Y. Bar-Cohen, Z. Chang et al., "Modeling and computer simulation of ultrasonic/sonic driller/corer (USDC)," *IEEE Transactions on Ultrasonics, Ferroelectrics, and Frequency Control*, vol. 50, no. 9, pp. 1147–1160, 2003.

[7] D. Bai, Q. Quan, Y. Wang, D. Tang, and Z. Deng, "A longitudinal & longitudinal-torsional vibration actuator for rotary-percussive ultrasonic planetary drills," *Advances in Space Research*, vol. 63, no. 2, pp. 1065–1072, 2019.

[8] Y. Wang, Q. Quan, H. Yu, D. Bai, H. Li, and Z. Deng, "Rotary-percussive ultrasonic drill: an effective subsurface penetrating tool for minor planet exploration," *IEEE Access*, vol. 6, pp. 37796–37806, 2018.

[9] X. Wang, X. Wang, J. Wang, and Z. Tian, "Feasibility study and prospects of rock fragmentation using ultrasonic vibration excitation," *Applied Sciences*, vol. 10, no. 17, p. 5868, 2020.

[10] L. Zhang, X. Wang, J. Wang, and Z. Yang, "Mechanical characteristics and pore evolution of red sandstone under ultrasonic high-frequency vibration excitation," *AIP Advances*, vol. 11, no. 5, Article ID 055202, 2021.

[11] P. K. S. C. Fernando, Z. J. Pei, and M. Zhang, "Mechanistic cutting force model for rotary ultrasonic machining of rocks," *International Journal of Advanced Manufacturing Technology*, vol. 109, no. 1-2, pp. 109–128, 2020.

[12] M. He, N. Li, Y. Chen, and C. Zhu, "Strength and fatigue properties of sandstone under dynamic cyclic loading," *Shock and Vibration*, vol. 2016, Article ID 9458582, 8 pages, 2016.

[13] Z. Zhou, H. Wang, X. Cai, L. Chen, Y. E, and R. Cheng, "Damage evolution and failure behavior of post-mainshock damaged rocks under aftershock effects," *Energies*, vol. 12, no. 23, p. 4429, 2019.

[14] H. Haghgouei, A. Baghbanan, H. Hashemolhosseini, and S. Jamali, "Variable amplitude fatigue life prediction of rock samples under completely reversed loading," *Geotechnical & Geological Engineering*, vol. 39, no. 3, pp. 1951–1962, 2021.

[15] B. Yang, M. He, and Y. Chen, "Experimental study of nonlinear damping characteristics on granite and red sandstone under the multi-level cyclic loading-unloading triaxial compression," *Arabian Journal of Geosciences*, vol. 13, no. 2, p. 72, 2020.

[16] M. Liao, Y. Liu, J. Paez Chavez, A. S. Chong, and M. Wiercigroch, "Dynamics of vibro-impact drilling with linear and nonlinear rock models," *International Journal of Mechanical Sciences*, vol. 146-147, pp. 200–210, 2018.

[17] Y. Wang, L. Ma, P. Fan, and Y. Chen, "A fatigue damage model for rock salt considering the effects of loading frequency and amplitude," *International Journal of Mining Science and Technology*, vol. 26, no. 5, pp. 955–958, 2016.

[18] Y. Zhou, Q. Sheng, N. Li, and X. Fu, "Numerical investigation of the deformation properties of rock materials subjected to cyclic compression by the finite element method," *Soil Dynamics and Earthquake Engineering*, vol. 126, Article ID 105795, 2019.

[19] X. Chen, C. A. Tang, and X. Kong, "Study on progressive damage and failure of sandstone samples subjected to cyclic disturbance loads using a modified triaxial test system," *KSCE Journal of Civil Engineering*, vol. 23, no. 5, pp. 2371–2383, 2019.

[20] H. Wang, M. He, J. Zhu, S. Guo, Y. Chen, and N. Li, "Experimental investigation of linear damping characteristics on granite and red sandstone under dynamic cyclic loading,"

European Journal of Environmental and Civil Engineering, vol. 26, no. 11, pp. 5259–5278, 2021.

[21] R. Geranmayeh Vaneghi, K. Thoeni, A. V. Dyskin, M. Sharifzadeh, and M. Sarmadivaleh, "Fatigue damage response of typical crystalline and granular rocks to uniaxial cyclic compression," *International Journal of Fatigue*, vol. 138, Article ID 105667, 2020.

[22] Z. Zhou, J. Zhang, X. Cai et al., "Permeability evolution of fractured rock subjected to cyclic axial load conditions," *Geofluids*, vol. 2020, Article ID 4342514, 12 pages, 2020.

[23] X. H. Zhu, Y. X. Luo, and W. Liu, "The rock breaking and ROP increase mechanisms for single-tooth torsional impact cutting using DEM," *Petroleum Science*, vol. 16, no. 5, pp. 1134–1147, 2019.

[24] J. Zhu, T. Zhai, Z. Liao, S. Yang, X. Liu, and T. Zhou, "Low-amplitude wave propagation and attenuation through damaged rock and a classification scheme for rock fracturing degree," *Rock Mechanics and Rock Engineering*, vol. 53, no. 9, pp. 3983–4000, 2020.

[25] K. Zhou, T. Liu, and Z. Hu, "Exploration of damage evolution in marble due to lateral unloading using nuclear magnetic resonance," *Engineering Geology*, vol. 244, pp. 75–85, 2018.

[26] T. Liu, C. Zhang, J. Li, K. Zhou, and C. Ping, "Detecting freeze–thaw damage degradation of sandstone with initial damage using NMR technology," *Bulletin of Engineering Geology and the Environment*, vol. 80, no. 6, pp. 4529–4545, 2021.

[27] S. Li, *Research on Rock Breaking Mechanism of Drill Bit under Harmonic Vibration Excitation*, Northeast Petroleum University, 2016.

[28] Y. H. Huang, S. Q. Yang, and W. L. Tian, "Cracking process of a granite specimen that contains multiple pre-existing holes under uniaxial compression," *Fatigue and Fracture of Engineering Materials and Structures*, vol. 42, no. 6, pp. 1341–1356, 2019.

[29] S. Q. Yang, W. L. Tian, Y. H. Huang, P. G. Ranjith, and Y. Ju, "An experimental and numerical study on cracking behavior of brittle sandstone containing two non-coplanar fissures under uniaxial compression," *Rock Mechanics and Rock Engineering*, vol. 49, no. 4, pp. 1497–1515, 2016.

[30] X. F. Li, H. B. Li, Y. Q. Liu, Q. Zhou, and X. Xia, "Numerical simulation of rock fragmentation mechanisms subject to wedge penetration for TBMs," *Tunnelling and Underground Space Technology*, vol. 53, pp. 96–108, 2016.

[31] M. Saadat and A. Taheri, "Modelling micro-cracking behaviour of pre-cracked granite using grain-based distinct element model," *Rock Mechanics and Rock Engineering*, vol. 52, no. 11, pp. 4669–4692, 2019.

[32] H. Huang and E. Detournay, "Discrete element modeling of tool-rock interaction II: rock indentation," *International Journal for Numerical and Analytical Methods in Geomechanics*, vol. 37, no. 13, pp. 1930–1947, 2013.

[33] Y. Zhou, D. Zhao, Q. Tang, and M. Wang, "Experimental and numerical investigation of the fatigue behaviour and crack evolution mechanism of granite under ultra-high-frequency loading," *Royal Society Open Science*, vol. 7, no. 4, Article ID 200091, 2020.

[34] J. G. Cai and J. Zhao, "Effects of multiple parallel fractures on apparent attenuation of stress waves in rock masses," *International Journal of Rock Mechanics and Mining Sciences*, vol. 37, no. 4, pp. 661–682, 2000.

[35] D. Zhao, S. Zhang, Y. Zhao, and M. Wang, "Experimental study on damage characteristics of granite under ultrasonic vibration load based on infrared thermography," *Environmental Earth Sciences*, vol. 78, no. 14, p. 419, 2019.

[36] B. Dai, Q. w. Shan, Y. Chen, and Xy Luo, "Mechanical and energy dissipation characteristics of granite under cyclic impact loading," *Journal of Central South University*, vol. 29, no. 1, pp. 116–128, 2022.